BIOCHEMISTRY
including biophysical chemistry & molecular biology

Article

pubs.acs.org/biochemistry

Conformational Activation of Poly(ADP-ribose) Polymerase-1 upon DNA Binding Revealed by Small-Angle X-ray Scattering

Steven O. Mansoorabadi,[†,∥] Meilan Wu,[†] Zhihua Tao,[†] Peng Gao,[†] Sai Venkatesh Pingali,[‡] Liang Guo,[§] and Hung-wen Liu*[,†]

[†]Division of Medicinal Chemistry, College of Pharmacy, Department of Chemistry, and Institute of Cellular and Molecular Biology, The University of Texas at Austin, Austin, Texas 78712, United States

[‡]Oak Ridge National Laboratory, Oak Ridge, Tennessee 37831, United States

[§]Advanced Photon Source, Argonne National Laboratory, Argonne, Illinois 60439, United States

Supporting Information

ABSTRACT: Poly(ADP-ribose) polymerase-1 (PARP-1) is a nuclear protein that plays key roles in several fundamental cellular processes. PARP-1 catalyzes the polymerization of nicotinamide adenine dinucleotide on itself and other acceptor proteins, forming long branched poly(ADP-ribose) polymers. The catalytic activity of PARP-1 is stimulated upon binding to damaged DNA, but how this signal is transmitted from the N-terminal DNA binding domain to the C-terminal catalytic domain in the context of the full-length enzyme is unknown. In this paper, small-angle X-ray scattering experiments and molecular dynamics simulations were used to gain insight into the conformational changes that occur during the catalytic activation of PARP-1 by an 8-mer DNA ligand. The data are consistent with a model in which binding of the DNA ligand establishes interdomain interactions between the DNA binding and catalytic domains, which induces an allosteric change in the active site that promotes catalysis. Moreover, the PARP-1−8-mer complex is seen to adopt a conformation that is poised to recruit DNA repair factors to the site of DNA damage. This study provides the first structural information about the DNA-induced conformational activation of full-length PARP-1.

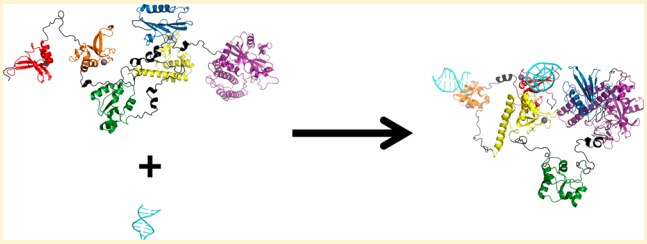

Poly(ADP-ribose) polymerase-1 (PARP-1) is an abundant nuclear protein that is implicated in many essential cellular processes, such as DNA damage repair and the regulation of chromatin structure and transcription.[1−3] PARP-1 is activated upon binding to damaged DNA and catalyzes the cleavage of nicotinamide adenine dinucleotide (NAD^+) to nicotinamide and ADP-ribose; the latter is covalently attached to nuclear acceptor proteins as a linear or branched polymer [poly(ADP-ribose) (PAR) (Scheme 1)].[4] Several protein substrates of PARP-1 have been identified, including histones, transcription factors, and PARP-1 itself.[5,6] Extensive poly(ADP-ribosyl)ation of PARP-1 (automodification) results in the downregulation of its enzymatic activity.[5] Inactivation of PARP-1 by caspase-3 cleavage is a key event in apoptosis, while overactivation of PARP-1 leads to the depletion of cellular ATP levels and necrosis.[7,8] Given the central role of PARP-1 in the maintenance of genomic stability and apoptosis, inhibitors of PARP-1 show much promise as novel therapeutics for the treatment of cancer and inflammatory diseases.[9−11]

PARP-1 is a 113 kDa protein consisting of three main functional domains: an N-terminal DNA binding domain, a central automodification domain, and a C-terminal catalytic domain.[12] These domains are further subdivided into smaller regions (domains A−F) that share homology with previously identified functional modules (Scheme 2). Domain A contains two unusual "PARP-like" zinc fingers (FI and FII).[13] A bipartite nuclear localization sequence (NLS) is located in domain B.[14] Domain C, which contains a novel zinc-ribbon motif, is required for the catalytic activation of PARP-1 upon DNA binding, though it does not itself bind to DNA; it does, however, have affinity for the PAR polymer.[15,16] Together, domains A−C form the N-terminal DNA binding domain. The automodification domain (domain D) contains a BRCT [breast cancer type 1 susceptibility protein (BRCA1) C-terminal] motif, which is known to be involved in the formation of protein−protein interactions.[17] Domain E, the WGR domain, which is named after the several conserved tryptophan, glycine, and arginine residues it contains, was identified as a potential nucleic acid binding domain and is known to have affinity for PAR polymers.[18,19] Recently, a double-stranded DNA binding (DsDB) domain was identified within the loop connecting the BRCT and WGR domains.[19] Domain F contains the so-called PARP regulatory domain (PRD) at its N-terminus and the PARP signature motif at its C-terminus; the latter houses the active site of PARP-1.[20,21] Domains E and F comprise the catalytic domain.

Received: October 22, 2013
Revised: January 31, 2014
Published: March 3, 2014

Scheme 1. Reaction Catalyzed by PARP-1

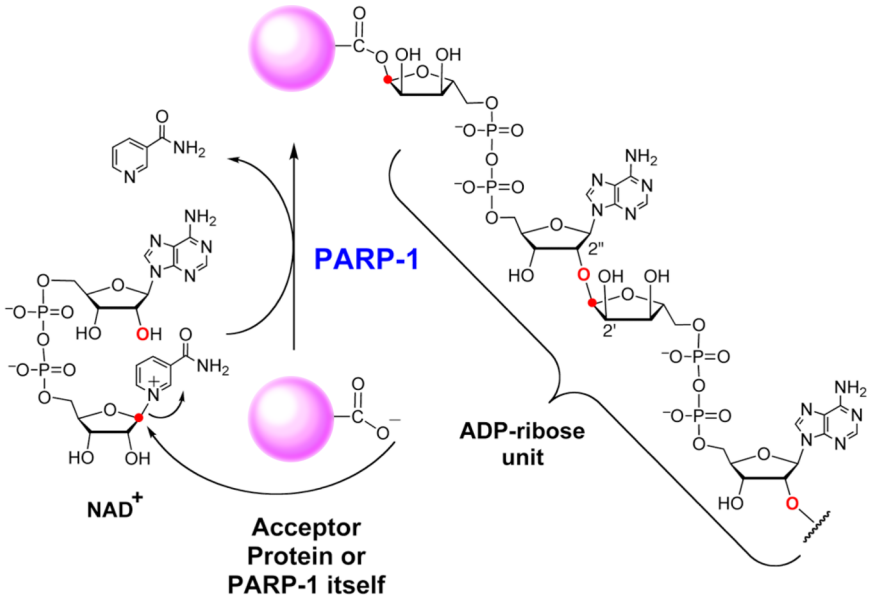

Scheme 2. Domain Structure of PARP-1

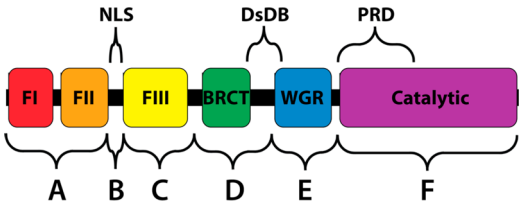

The high-resolution structures of most of the individual domains of human PARP-1 are known,[15,16,22−28] though it is still unclear how these domains are organized into a functional whole. Recently, FI and domain C were cocrystallized with the catalytic domain in the presence of DNA.[29] However, the structure of full-length PARP-1 in the presence or absence of DNA has thus far eluded analysis by NMR spectroscopy or X-ray crystallography, in part because of the large size and high degree of flexibility of the enzyme. Small-angle X-ray scattering (SAXS) is a powerful technique that can be used to probe the low-resolution solution structures of such systems.[30] In this paper, the structural changes of full-length PARP-1 (as well as that of several domain deletion mutants) associated with binding to an 8-mer DNA ligand known to induce poly(ADP-ribosyl)ation activity[31] were analyzed using SAXS and molecular dynamics simulations to gain insight into the catalytic activation mechanism of PARP-1.

MATERIALS AND METHODS

Cloning, Expression, and Purification of PARP-1 Constructs. DNA encoding residues 1−232 [domains A and B (AB)], 1−373 [domains A−C (ABC)], 369−1014 [domains D−F (DEF)], or 1−1014 (full-length PARP-1) of the human PARP-1 enzyme was cloned into the MalE-pET expression vector at the NdeI and XhoI restriction sites. MalE-pET is a modified pET-24b(+) vector designed to express the PARP-1 constructs with an N-terminal decahistidine-maltose binding protein (MBP) tag and an intervening TEV protease cleavage site.[16] The DEFΔ mutant, which lacks residues 626−645 at the C-terminal end of the WGR domain, was constructed using the QuikChange Site-directed Mutagenesis Kit (Stratagene), with 5′-CAC TTC ATG AAA TTA TAT GAA GAA AAA ACC GGG AAC GCT GGC CAG GAT GAA GAG-3′ and 5′-CTC TTC ATC CTG GCC AGC GTT CCC GGT TTT TTC TTC ATA TAA TTT CAT GAA GTG-3′ as the primers and the DEF/MalE-pET plasmid as the template. To construct the full-length PARP-1Δ mutant (also lacking residues 626−645), the DEFΔ/MalE-pET and PARP-1/MalE-pET plasmids were digested with the PstI and XhoI restriction enzymes. The small DNA fragment from the former and the large DNA fragment from the latter restriction digestion reactions were gel purified and ligated together to generate the PARP-1Δ/MalE-pET plasmid. The sequence of the resulting PARP-1Δ/MalE-pET plasmid was verified by DNA sequencing at the DNA Sequencing Core Facility at The University of Texas at Austin.

The MalE-pET vectors containing the PARP-1 constructs were transformed into *Escherichia coli* Rosseta2 BL21(DE3) (Novagen) and grown at 37 °C in 6 L of Luria-Bertani broth containing 50 μg/mL kanamycin. Expression of the MBP-tagged PARP-1 constructs was induced by the addition of 0.2 mM IPTG when the OD_{600} of the cultures reached 0.5. The cultures were grown for an additional 20 h at 18 °C, and the cells were harvested by centrifugation (7000*g* for 10 min) and stored at −80 °C until they were further used.

The PARP-1 constructs were purified according to the procedure previously described for domain C with a few modifications.[16] Briefly, thawed cells were resuspended in lysis buffer containing 20 mM HEPES, 300 mM NaCl, 10 mM imidazole, 1 mM β-mercaptoethanol, and 10% glycerol (pH 7.5) and sonicated. Cell debris was removed by centrifugation at 18000*g* for 30 min, and the resulting supernatant was incubated with 10 mL of Ni-NTA agarose resin (Qiagen) at 4 °C for 1 h. The mixture was loaded onto a column, allowed to drain, and then washed with lysis buffer. The column was then washed extensively with lysis buffer containing 1 M NaCl. The MBP fusion proteins were then eluted from the column with lysis buffer containing 0.25 M imidazole. The desired protein fractions were pooled and dialyzed against lysis buffer. During dialysis, the fusion proteins were incubated with 2% (w/w) His_6-TEV protease to cleave the His_{10}-MBP tag, leaving behind

dx.doi.org/10.1021/bi401439n | *Biochemistry* 2014, 53, 1779−1788

two additional amino acid (Gly-His) residues at the N-terminus of the corresponding PARP-1 construct. The constructs were then purified from His_{10}-MBP and His_6-TEV protease by slowly filtering the mixture through a column containing 10 mL of Ni-NTA resin. The flow-through was concentrated with an Amicon concentrator using a YM 10 membrane (Millipore) and further purified by size exclusion chromatography using an AKTA FPLC system and a Superdex 200 column (GE Healthcare). The elution buffer contained 20 mM HEPES, 300 mM NaCl, and 10% glycerol (pH 7.5). Fractions containing the desired PARP-1 constructs [as judged by sodium dodecyl sulfate−polyacrylamide gel electrophoresis (SDS−PAGE)] were pooled and concentrated as described above.

Preparation of DNA Ligands. Single-stranded 8-mer (5′-GGA ATT CC-3′) and 44-mer (5′-CGG TCG ATC GTA AGA TCG ACC GGC GCT GGA GCT TGC TCC AGC GC-3′) DNA were purchased from IDT DNA Co. (Coralville, IA). To prepare the corresponding double-stranded 8-mer and 44-mer nicked dumbbell DNA ligands, the oligos were dissolved in annealing buffer containing 100 mM NaCl and 10 mM Tris-HCl (pH 7.5). The samples were then heated to 95 °C for 4 min, cooled slowly to 4 °C, and dialyzed into buffer containing 20 mM HEPES, 300 mM NaCl, and 10% glycerol (pH 7.5).

SAXS Data Collection and Processing. Synchrotron X-ray scattering data from solutions of PARP-1 constructs were obtained with BioCAT beamline 18 ID (Advanced Photon Source, Argonne National Laboratory), equipped with a high-sensitivity Aviex CCD detector. Samples (~120 μL) were housed in a water-jacket flow cell maintained at 4 °C. For samples containing both protein and DNA, the PARP-1 constructs were incubated with DNA at either a 1:1 (AB and ABC) or a 1:2 (full-length PARP-1) molar ratio. The sample concentrations were as follows: 8-mer DNA, 0.15 mg/mL; AB, 0.80 mg/mL; AB−8-mer, 0.77 mg/mL; ABC, 1.7 mg/mL; ABC−8-mer, 1.6 mg/mL; DEF, 1.5 mg/mL; PARP-1, 0.47 mg/mL; PARP-1−8-mer, 0.46 mg/mL. All samples were centrifuged continuously at 4 °C in a microcentrifuge prior to data collection. The samples were passed through the 12 keV X-ray beam using a Hamilton programmable dual-syringe pump 3 m from the detector, which minimized radiation damage and allowed a Q range of scattering vectors of 0.06−4 nm^{-1} to be covered. Fifteen 6 s frames of scattering data were collected for each sample and the corresponding buffer control. Frames showing evidence of radiation damage were discarded, and those remaining were averaged. The average scattering curves were then normalized to the intensity of the incident X-ray beam, and the background scattering of the buffer was subtracted. The difference curves were then extrapolated to infinite dilution using PRIMUS.[32]

SAXS Data Analysis and Model Building. The forward scattering [$I(0)$], pair distribution function [$P(r)$], radius of gyration (R_g), and maximal dimension (D_{max}) of each PARP-1 construct were evaluated by indirect Fourier transformation using the AUTOGNOM software package.[33] DAMMIN verion 53 was then used for *ab initio* shape determination of each construct.[34] This program utilizes a simulated annealing algorithm to produce a single-phase dummy atom model that best reproduces the experimental scattering curves, subjected to looseness penalties for the calculated structure. For each PARP-1 construct, 100 DAMMIN reconstructions were performed and the 20 structures with the smallest χ values with respect to the experimental curves were averaged.

CORAL was used to obtain structural models of the PARP-1 constructs and their complexes with 8-mer DNA using the available high-resolution domain structures.[35] In this program, the position and orientation of each domain and/or subunit and the conformation of any intervening linkers (modeled as a chain of dummy residues with a spacing of 3.8 Å) are varied simultaneously to determine the structure that best reproduces the SAXS data. A simulated annealing algorithm is employed for the minimization protocol, which includes penalties for steric clashes and improper loop conformations. The high-resolution structures utilized in the calculations were as follows: 8-mer DNA (PDB entry 4DQY or 3ODC), zinc finger I (FI, residues 6−91, PDB entry 4DQY), zinc finger II (FII, residues 113−198, PDB entry 3ODC), zinc finger III (FIII, residues 224−359, PDB entry 4DQY), BRCT domain (residues 388−483, PDB entry 2COK), WGR domain (residues 531−644, PDB entry 4DQY), and catalytic domain (residues 662−1009, PDB entry 4DQY).[22,23,29] SABBAC (online Structural Alphabet-based protein BackBone reconstruction from Alpha-Carbon trace)[36] was then utilized to position the missing atoms in the flexible linkers of the structural models of full-length PARP-1 and the PARP-1−8-mer complex generated by CORAL. This program uses the coordinates of the α-carbons of a protein to select candidate fragments from a Hidden Markov Model-derived structural alphabet and assembles the fragments using a greedy algorithm to reconstruct the peptide chain.

Molecular Dynamics Simulations. Molecular dynamics simulations were then used to energy minimize and equilibrate the structures of full-length PARP-1 and the PARP-1−8-mer complex from CORAL using NAMD version 2.9. NAMD was developed by the Theoretical and Computational Biophysics Group in the Beckman Institute for Advanced Science and Technology at the University of Illinois at Urbana-Champaign.[37] The protonation states of histidine residues and the cysteine residues coordinated to the zinc ions were selected to reflect their local environments. The PARP-1 molecules were placed in a box of solvent water modeled with the TIP3P parameters, with a box padding of 15 Å. Sodium and chloride ions were added to adjust the ionic strength of the solvent to 0.6 M and neutralize the system. The CHARMM27 force field was used for protein and nucleic acid parameters. A switching distance of 10 Å, a cutoff of 12 Å, and a pair list distance of 14 Å were used for electrostatic and van der Waals interactions. The simulations used a 2 fs time step size, with rigid bonds enabled for all atoms. Nonbonded and full electrostatic forces were evaluated at each step and every other step, respectively. Periodic boundary conditions were employed, with the particle mesh Ewald sum method being utilized for long-range electrostatic interactions. The temperatures of the systems were held constant at 277.15 K using Langevin dynamics for all non-hydrogen atoms and a damping coefficient of 5 ps. The pressures were maintained at 1.01325 bar using a Nosé-Hoover Langevin piston with oscillation and damping time constants of 200 and 100 fs, respectively. The systems were first minimized for 5000 steps (10 ps) and then equilibrated for 250000 steps (0.5 ns).

Electrophoretic Mobility Shift Assay. The relative DNA binding affinities of DEF and PARP-1, as well as the corresponding deletion mutants lacking residues 626−645 in the WGR domain (DEFΔ and PARP-1Δ), were measured using an electrophoretic mobility shift assay (EMSA). The DNA ligand (150 pmol of 8-mer or nicked dumbbell DNA)

was incubated with the PARP-1 constructs at various protein:DNA ratios (0:1, 1:1, 2:1, 3:1, 4:1, 5:1, and 6:1) in a total volume of 8 μL. The samples were allowed to equilibrate on ice for 30 min, after which they were run on a 1.5% agarose gel and visualized using ethidium bromide staining and UV transillumination.

Automodification Assay. The automodification activities of full-length PARP-1 and the PARP-1Δ mutant were analyzed using an SDS−PAGE assay. Reactions of 1 μM enzyme, 1 μM 8-mer DNA, 5 mM NAD^+, 50 mM NaCl, 7.5 mM $MgCl_2$, and 20 mM Tris buffer (pH 7.5) were quenched at various time points using 2× SDS−PAGE loading buffer containing 50 mM EDTA. Reactions were initiated by the addition of NAD^+. As a negative control, 8-mer DNA was omitted from the mixtures, and the reaction was quenched after 5 min. After the reaction had been quenched, the automodified PARP-1 constructs were separated from the unmodified enzyme on an SDS−PAGE gel and visualized by being stained with Coomassie Brilliant Blue.

RESULTS AND DISCUSSION

The experimental SAXS data of the PARP-1 constructs (AB, ABC, DEF, and full-length PARP-1) and the 8-mer DNA ligand are shown in Figure 1. GNOM analysis of the SAXS data

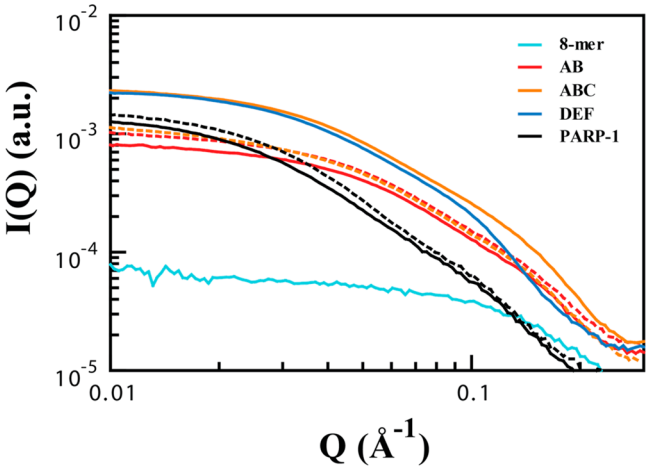

Figure 1. SAXS intensity as a function of momentum transfer for all PARP-1 constructs and the DNA ligand used in this study. SAXS data of PARP-1 constructs bound to 8-mer DNA are indicated with a dotted line.

yielded estimates for the forward scattering [$I(0)$], radius of gyration (R_g), maximal dimension (D_{max}), and pair distribution function [$P(r)$] for each construct (Table 1 and Figure S1 of the Supporting Information).[33] The pair distribution functions

Table 1. R_g and D_{max} Estimates from GNOM for Fits to the SAXS Data

construct	$I(0)$ (×10^5)	R_g (Å)	D_{max} (Å)
8-mer	5.736	11.56	39.00
AB	75.59	27.99	86.09
AB−/8-mer	93.52	29.20	89.96
ABC	232.3	37.53	113.8
ABC−8-mer	108.8	37.64	142.0
DEF	231.9	40.64	126.8
PARP-1	136.3	56.74	176.2
PARP-1−8-mer	151.6	51.90	160.6

for the PARP-1 domain deletion mutants (AB, ABC, and DEF) contain several distinct maxima, consistent with the presence of individual ordered domains connected by flexible linkers. The $P(r)$ for the AB construct (residues 1−232) was similar to that obtained in a previous SAXS study of domain A (residues 1−209).[38] Upon binding to 8-mer DNA, full-length PARP-1 undergoes a conformational change in which its structure become more compact. This can be seen in the smaller R_g and D_{max} value for the DNA complex (Table 1) or by comparison of the corresponding pair distribution functions (Figure S1 of the Supporting Information).

In contrast to these observations, the AB and ABC constructs become more elongated upon DNA binding (Table 1 and Figure S1 of the Supporting Information). In addition, the previous SAXS study demonstrated that the binding of 30-mer blunt DNA to domain A or the ABCD construct (residues 1−486) resulted in more elongated structures.[38] A more elongated structure can be expected when DNA binds to the relatively small zinc finger containing constructs of PARP-1 (i.e., A or AB). However, it was surprising that full-length PARP-1 became more compact upon DNA binding, while the ABC and ABCD constructs were elongated. This result may be explained by the absence of the WGR domain, and the majority of the loop connecting it to the BRCT domain, in the ABC and ABCD constructs. The WGR domain has been suggested to be a potential nucleic acid binding motif, and the loop connecting the WGR and BRCT domains (residues 480−540) has recently been shown to be a double-stranded DNA binding (DsDB) domain.[18,19] Thus, these data suggest that the activation of PARP-1 by damaged DNA may involve a conformational change in which both the zinc finger and the WGR and DsDB domains form contacts with the DNA ligand.

The solution structures of the PARP-1 constructs were modeled using DAMMIN and CORAL. DAMMIN generates an *ab initio* dummy atom model of the low-resolution molecular shape of each construct.[34] In contrast, CORAL utilizes the available high-resolution structural data of the individual domains (and DNA ligands) and builds in the missing linkers using a chain of dummy residues.[35] Superpositions of these models for the PARP-1 constructs are shown in Figure 2, and the associated χ values for fits to the experimental SAXS data are summarized in Table 2. The molecular shape of the 8-mer DNA ligand was also reconstructed using DAMMIN, and the resulting low-resolution structure was aligned with an average B-form DNA duplex generated using the Nucleic Acid Builder (NAB) programming language (Figure 2).[40]

The structure of the PARP-1−8-mer complex was modeled in two ways using CORAL (Figure 3). In the first model (χ = 1.93), the FI, C, and EF domains were fixed in the same orientation observed in the cocrystal structure.[29] This results in domain D (the automodification domain) being placed adjacent to the catalytic domain, in a position conducive for the poly(ADP-ribosyl)ation of several recently identified automodification sites (D387, E488, and E491).[41] These modification sites reside in the loops connecting domain D to domains C and E, which could bind to the active site housing the catalytic base E988 via a conformational change.[42] The constraints imposed on domains FI, C, and EF were relaxed in the second model, which resulted in a significantly better fit to the experimental SAXS data (χ = 0.58). Interestingly, the automodification domain D is found in a dramatically different position in this model (Figure 3). Domain D also contains a

dx.doi.org/10.1021/bi401439n | *Biochemistry* 2014, 53, 1779−1788

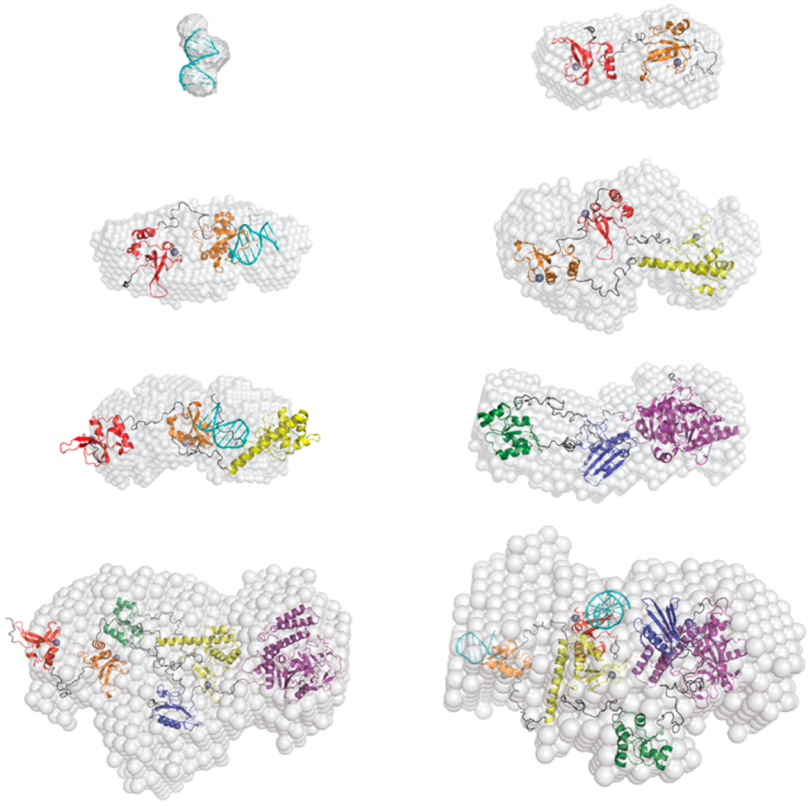

Figure 2. Comparison of DAMMIN reconstructions of the PARP-1 constructs and the 8-mer DNA ligand with the corresponding models obtained using CORAL or NAB. Structural superpositions were achieved using SUPCOMB20.[39] Individual PARP-1 domains are colored as in Scheme 2, and the 8-mer DNA is colored cyan. The chains of dummy residues connecting the PARP-1 domains in the CORAL models are shown as black loops. Zinc ions are shown as gray spheres. Constructs from top left to bottom right 8-mer DNA, AB, AB−8-mer, ABC, ABC−8-mer, DEF, PARP-1, and PARP-1−8-mer, respectively. All ribbon representations and dummy atoms are shown to scale.

Table 2. χ Values for Fits to Experimental SAXS Data

construct	DAMMIN	CORAL
8-mer	0.412−0.413	–
AB	0.775−0.842	0.75
AB−8-mer	0.619−0.667	0.59
ABC	1.392−1.708	1.12
ABC−8-mer	1.638−2.322	1.27
DEF	1.140−1.384	0.94
PARP-1	0.822−1.194	0.49
PARP-1−8-mer	0.568−0.747	0.58

BRCT motif, which is known to be involved in forming protein−protein interactions. Upon binding to and being activated by damaged DNA, PARP-1 recruits DNA repair factors to the lesion site, specifically X-ray cross complementing group 1 protein (XRCC1), which is a DNA repair scaffolding protein. Recently, it was shown that PARP-1 does not interact significantly with XRCC1 unless it has been automodified.[43] Moreover, the loop connecting domains D and E contains the double-stranded DNA binding (DsDB) domain, which in this structural model would be positioned such that it could bind to the double-stranded region of DNA adjacent to a lesion site in genomic DNA. It is therefore tempting to speculate that the best-fit structural model of the PARP-1−8-mer complex is in a conformation that resembles the one that recruits XRCC1 to the site of DNA damage after PARP-1 automodification.

SABBAC was then used to reconstruct the peptide backbone and position the side chains of the amino acid residues within the flexible linkers of the best-fit structural models of full-length PARP-1 and the PARP-1−8-mer complex generated by CORAL.[35,36] The resulting PARP-1−8-mer structure and that of unliganded PARP-1 were then subjected to energy minimization and equilibration in a box of water using molecular dynamics simulations as implemented in the NAMD software package.[37] A comparison of the structures of PARP-1 and the PARP-1−8-mer complex obtained after a 10 ps energy minimization and a 0.5 ns equilibration is shown in Figure 4.

When full-length PARP-1 binds to DNA, the most dramatic conformational changes to its structure, not surprisingly, occur in the DNA binding domain. Both FI and FIII (as well as the WGR domain) form interdomain contacts with the catalytic domain via the PARP regulatory domain (PRD).[20,21] FI is known to be critical for DNA-dependent activation of PARP-1, while FII is dispensable for this purpose even though it has a greater affinity for DNA.[22,44−47] In particular, mutations to one of several residues in FI (Q40, D45, L77, and K97) were shown to eliminate activation of the poly(ADP-ribosyl)ation activity of PARP-1 in the presence of DNA, despite the fact that these mutants could still bind DNA with an affinity similar to that of the wild-type enzyme (Figure 5).[22,44] Similarly, mutational studies showed several residues in FIII to be critical for DNA-dependent enzyme activation but not DNA binding (K249, G313, T316, and W318) (Figure 5).[44] It is therefore likely that these interdomain interactions with the PRD induce an allosteric change in the catalytic domain that stimulates the poly(ADP-ribosyl)ation activity of PARP-1. In support of this

dx.doi.org/10.1021/bi401439n | *Biochemistry* 2014, 53, 1779−1788

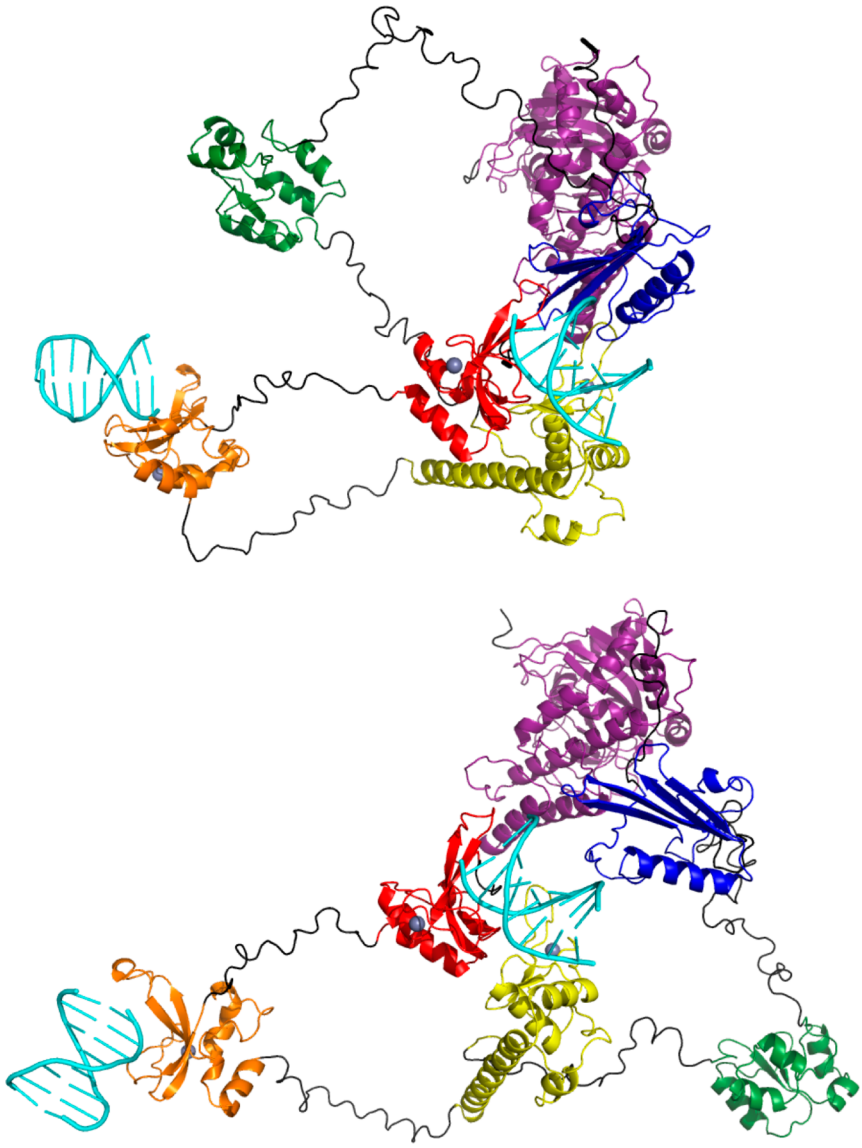

Figure 3. Comparison of the CORAL structural models of the PARP-1−8-mer complex obtained by fixing the FI, C, and EF domains in the positions observed in the cocrystal structure (top) or after relaxing these constraints (bottom).[29] The later model results in significantly better fits (χ = 0.58) to the experimental SAXS data (χ = 1.93) and a dramatically different position of the BRCT domain (green) relative to the DNA binding and catalytic domains. The PARP-1−8-mer models were aligned using SUPCOMB20.[39] The structures are rendered and colored as described in the legend of Figure 2.

hypothesis, a gain-of-function mutant containing an L713F substitution in the PRD was previously identified and found to increase the k_{cat} and k_{cat}/K_M ~10-fold relative to that of the wild-type enzyme (Figure 5).[48] In addition, this increase in catalytic activity was observed in the basal activity of the catalytic domain, independent of DNA binding.[48] Thus, this amino acid substitution may elicit a structural change in the active site that mimics the allosteric activation observed upon DNA binding. In addition, there are several phosphorylation sites in the DNA binding (S32, S41, S177, S179, S257/T258, and T335) and catalytic (S542, T656, Y775, S782, and S785/S786) domains that may modulate the interdomain interactions that activate PARP-1.[49]

Another striking feature of the structure of the PARP-1−8-mer complex is that FII extends away from the core domains required for DNA-dependent poly(ADP-ribosyl)ation activity (FI, FIII, and EF) (Figure 4). The two 8-mer ligands are bound to FI and FII such that their helical axes are approximately orthogonal to one another. As mentioned above, FII imparts PARP-1 with most of its DNA binding affinity.[22,45−47] FII is connected to the core domains through two flexible linkers, which likely is important for the ability of PARP-1 to recognize and be activated by a large number of DNA structures,[50] including nicked DNA,[51,52] double-strand breaks,[53] overhangs,[54] cruciforms,[55,56] and promoter regions.[57] The WGR domain also forms contacts with DNA in the structural model of the PARP-1−8-mer complex. To obtain experimental evidence of this predicted interaction, a deletion mutant of the DEF construct lacking residues 626−645 at the C-terminal end of the WGR domain was constructed and tested for its ability to bind DNA. As shown in the EMSA data in Figure S2 of the Supporting Information, the affinity of the DEFΔ mutant for dumbbell DNA is clearly diminished compared to that of wild-type DEF. Similar results were obtained using 8-mer DNA (Figure S2 of the Supporting Information). Within the context of the full-length enzyme, the effect of deletion of residues

dx.doi.org/10.1021/bi401439n | *Biochemistry* 2014, 53, 1779−1788

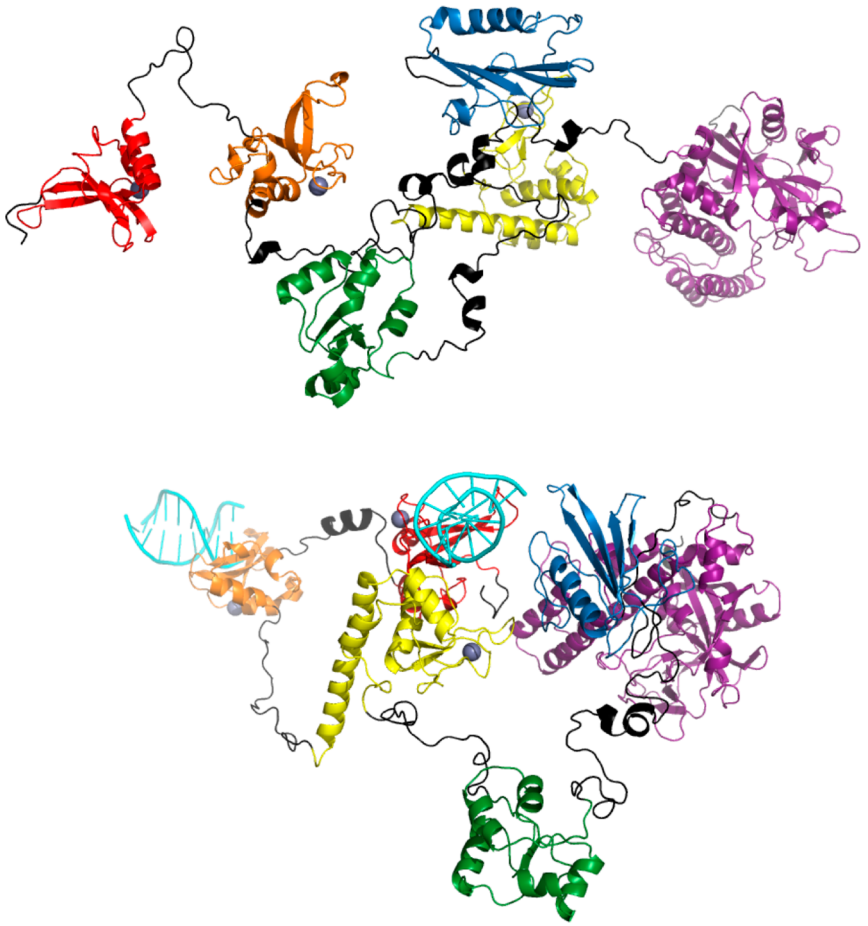

Figure 4. Conformational changes in the PARP-1 structural model upon binding to 8-mer DNA. Domain reorganization occurs as PARP-1 binds to 8-mer DNA, such that FI, domain C, and the WGR domain form contacts with the PARP regulatory domain (PRD). The PARP-1 (top) and PARP-1−8-mer (bottom) models were aligned using SUPCOMB20.[39] The structures are rendered and colored as described in the legend of Figure 2.

626−645 in the WGR domain on the DNA binding affinity of PARP-1 is less dramatic (Figure S3 of the Supporting Information). However, this deletion almost completely abolishes the automodification activity of PARP-1 (Figure S4 of the Supporting Information). Together, these data show that the WGR domain plays a critical role in the DNA-dependent activation of the poly(ADP-ribosyl)ation activity of PARP-1.

The DsDB domain is housed in the loop connecting domains D and E.[19] In the structure of the PARP-1−8-mer complex, the DsDB domain is positioned such that it can bind to DNA adjacent to a lesion site within genomic DNA, as is the loop connecting domains C and D. The DsDB domain contains a SUMOylation site (K486) and several lysine residues that have been identified as acetylation (and possible automodification) sites (K498, K505, K508, K521, and K524) (Figure 5).[58−60] PARP-1 is acetylated by the histone acetyltransferase p300 and its homologue, the cAMP-response element binding protein (CREB) binding protein (CBP).[59] Acetylation of PARP-1 is required for its function as a transcriptional coactivator of certain transcription factors (e.g., nuclear factor κB, NF-κB).[59] In addition, acetylation was shown to induce PARP-1 activation in the absence of DNA.[61] SUMOylation of PARP-1 by small ubiquitin-like modifier SUMO1 or SUMO3 abrogates p300/CBP-mediated acetylation of PARP-1 but has no effect on its DNA-dependent activation.[58] There are also several putative phosphorylation sites in the DsDB domain (S504 and S519), the BRCT domain (T420/T422 and S455), FIII (S257/T258 and T335), and the loop connecting the latter two domains (T368/S372/T373/S375) (Figure 5).[49] S372 and T373 were shown to be phosphorylated by the extracellular signal-regulated kinases ERK1 and ERK2, and this post-translational modification was found to increase the level of DNA-dependent PARP-1 activation.[62] These post-translational modifications undoubtedly have a profound influence on the specificity of PARP-1 for its substrate proteins and interaction partners and may also influence the DNA binding affinity and conformational dynamics of PARP-1 (e.g., interconversion of PARP-1 structures shown in Figures 3 and 4).

In summary, insight into the catalytic activation of PARP-1 by damaged DNA has been obtained from analysis of the SAXS data of the full-length enzyme and several truncation mutants. GNOM analysis of the SAXS data indicates that full-length PARP-1 and the AB and ABC constructs undergo conformational changes upon binding to DNA, wherein the former becomes more compact and the later two truncation mutants become elongated. The PARP-1 constructs and their associated DNA complexes are dynamic structures in solution, containing individual ordered domains connected by flexible linkers. Structural models of the PARP-1 constructs in the presence or absence of DNA were obtained from the SAXS data using CORAL. The structural models obtained from this analysis for full-length PARP-1 and the PARP-1−8-mer complex were further refined using molecular dynamics simulations. The structure of the PARP-1−8-mer complex is in a conformation

dx.doi.org/10.1021/bi401439n | *Biochemistry* 2014, 53, 1779−1788

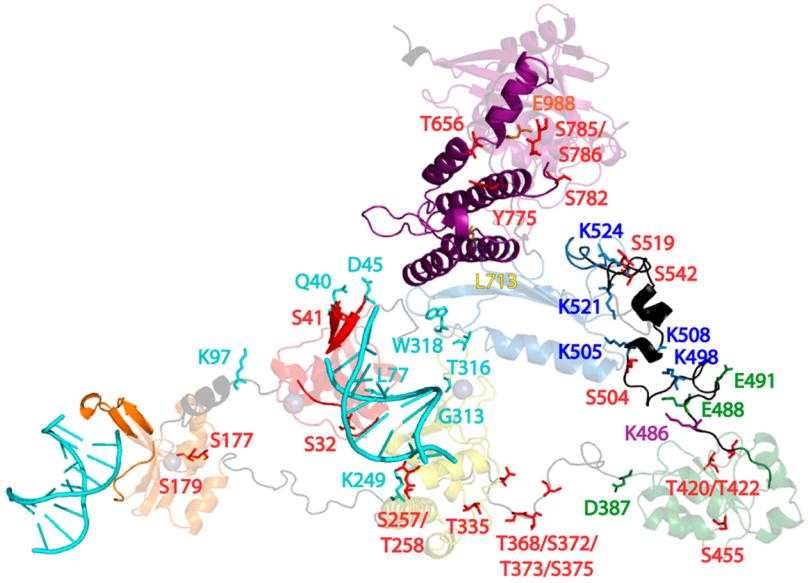

Figure 5. Positions of post-translational modification sites and functionally important residues identified via mutational analysis mapped on the PARP-1−8-mer structural model. The phosphate backbone grips and base stacking loops of FI and FII,[22] the double-stranded DNA binding domain (DsDB),[19] and the PARP regulatory domain (PRD)[20] are highlighted. Residues discussed in the text are labeled. Automodification sites: D387, E488, and E491 (green).[41] Phosphorylation sites: S32, S41, S177, S179, S257/T258, T335, T368/S372/T373/S375, T420/T422, S455, S504, S519, S542, T656, Y775, S782, and S785/S786 (red).[49] SUMOylation site: K486 (purple).[58] Acetylation/automodification sites: K498, K505, K508, K521, and K524 (blue).[59,60] Residues critical for DNA-dependent PARP activation but not DNA binding: Q40, D45, L77, K97, K249, G313, T316, and W318 (cyan),[22,44] Gain-of-function mutant residue: L713 (yellow).[48] Catalytic base required for poly(ADP-ribosyl)ation activity: E988 (orange).[42]

that appears to be poised to recruit DNA repair factors to the site of DNA damage. Comparison of the resulting PARP-1−8-mer atomistic model with that of free PARP-1 led to a working model of DNA-dependent PARP-1 activation. Specifically, PARP-1 binds to the site of DNA damage, which facilitates the formation of interdomain interactions between the DNA binding and catalytic domains that induce an allosteric change in the active site and stimulates poly(ADP-ribosyl)ation activity. This model is consistent with the results of previous structural and functional studies of the PARP-1 domains and with biochemical data for the residues and post-translational modifications important for DNA-dependent enzyme activation. In particular, the WGR domain plays a key role in the activation of PARP-1 poly(ADP-ribosyl)ation activity by interacting with both DNA (via its α-helix and central β-sheet) and the catalytic domain.[29] In this study, the WGR domain in the structural model of full-length PARP-1 is rotated out such that it is approximately perpendicular to its position in the crystal structure of the FI−C−EF−DNA complex[29] and is found to interact with 8-mer DNA via a loop at the C-terminal end of this domain. Deletion of residues 626−645 from this loop diminishes the DNA binding affinity of the catalytic domain and abolishes the automodification activity of PARP-1. This study provides, for the first time, structural information about the full-length enzyme and its complex with DNA and provides a framework from which to interpret new data to better understand the function and mechanism of this intriguing and centrally important nuclear enzyme.

■ ASSOCIATED CONTENT

Ⓢ Supporting Information

Supplementary Figures S1−S4. This material is available free of charge via the Internet at http://pubs.acs.org.

■ AUTHOR INFORMATION

Corresponding Author

*E-mail: h.w.liu@mail.utexas.edu. Telephone: (512) 232-7811. Fax: (512) 471-2746.

Present Address

‖S.O.M.: Department of Chemistry and Biochemistry, Auburn University, Auburn, AL 36849.

Funding

This work was supported by funding from the Texas Institute for Drug and Diagnostic Development (TI-3D) of The University of Texas at Austin, the Welch Foundation (F-1511), the National Institutes of Health (NIH) National Center for Research Resources (NCRR), the Department of Energy (DOE) Office of Basic Energy Science (BES), and NIH Fellowship GM082085 awarded to S.O.M.

Notes

The authors declare no competing financial interest.

■ ACKNOWLEDGMENTS

We thank Dr. Pappannan Thiyagarajan for helpful discussions and assistance in collecting SAXS data on BioCAT beamline 18 ID at the Advanced Photon Source.

■ ABBREVIATIONS

BRCT, breast cancer type 1 susceptibility protein C-terminal; CBP, cAMP-response element binding protein (CREB) binding protein; CCD, charge-coupled device; DsDB, double-stranded DNA binding; ERK, extracellular signal-regulated kinase; FI, PARP-like zinc finger domain I; FII, PARP-like zinc finger domain II; FPLC, fast protein liquid chromatography; HEPES, 4-(2-hydroxyethyl)-1-piperazineethanesulfonic acid; IPTG, isopropyl β-D-1-thiogalactopyranoside; MBP, maltose binding protein; NAD, nicotinamide adenine dinucleotide; NF-κB, nuclear factor κB; NLS, nuclear localization sequence;

NMR, nuclear magnetic resonance; NTA, nitrilotriacetic acid; PARP-1, poly(ADP-ribose) polymerase-1; PDB, Protein Data Bank; PRD, PARP regulatory domain; SAXS, small-angle X-ray scattering; TEV, tobacco etch virus; WGR, tryptophan-glycine-arginine; XRCC1, X-ray cross complementing group 1 protein.

REFERENCES

(1) Satoh, M. S., and Lindahl, T. (1992) Role of poly(ADP-ribose) formation in DNA repair. *Nature 356*, 356−358.

(2) Kraus, W. L., and Lis, J. T. (2003) PARP goes transcription. *Cell 113*, 677−683.

(3) Krishnakumar, R., and Kraus, W. L. (2010) The PARP side of the nucleus: Molecular actions, physiological outcomes, and clinical targets. *Mol. Cell 39*, 8−24.

(4) Kim, M. Y., Zhang, T., and Kraus, W. L. (2005) Poly(ADP-ribosyl)ation by PARP-1: 'PAR-laying' NAD^+ into a nuclear signal. *Genes Dev. 19*, 1951−1967.

(5) D'Amours, D., Desnoyers, S., D'Silva, I., and Poirier, G. G. (1999) Poly(ADP-ribosyl)ation reactions in the regulation of nuclear functions. *Biochem. J. 342*, 249−268.

(6) Tao, Z., Gao, P., and Liu, H.-W. (2009) Studies of the expression of human poly(ADP-ribose) polymerase-1 in *Saccharomyces cerevisiae* and identification of PARP-1 substrates by yeast proteome microarray screening. *Biochemistry 48*, 11745−11754.

(7) Kaufmann, S. H., Desnoyers, S., Ottaviano, Y., Davidson, N. E., and Poirier, G. G. (1993) Specific proteolytic cleavage of poly(ADP-ribose) polymerase: An early marker of chemotherapy-induced apoptosis. *Cancer Res. 53*, 3976−3985.

(8) Martin, D. S., Bertino, J. R., and Koutcher, J. A. (2000) ATP depletion + pyrimidine depletion can markedly enhance cancer therapy: Fresh insight for a new approach. *Cancer Res. 60*, 6776−6783.

(9) Annunziata, C. M., and O'Shaughnessy, J. (2010) Poly(ADP-ribose) polymerase as a novel therapeutic target in cancer. *Clin. Cancer Res. 16*, 4517−4526.

(10) Peralta-Leal, A., Rodríguez-Vargas, J. M., Aguilar-Quesada, R., Rodríguez, M. I., Linares, J. L., de Almodóvar, M. R., and Oliver, F. J. (2009) PARP inhibitors: New partners in the therapy of cancer and inflammatory diseases. *Free Radical Biol. Med. 47*, 13−26.

(11) Giansanti, V., Donà, F., Tillhon, M., and Scovassi, A. I. (2010) PARP inhibitors: New tools to protect from inflammation. *Biochem. Pharmacol. 80*, 1869−1877.

(12) Kameshita, I., Matsuda, Z., Taniguchi, T., and Shizuta, Y. (1984) Poly(ADP-Rribose) synthetase. Separation and identification of three proteolytic fragments as the substrate-binding domain, the DNA-binding domain, and the automodification domain. *J. Biol. Chem. 259*, 4770−4776.

(13) Petrucco, S., and Percudani, R. (2008) Structural recognition of DNA by poly(ADP-ribose)polymerase-like zinc finger families. *FEBS J. 275*, 883−893.

(14) Schreiber, V., Molinete, M., Boeuf, H., de Murcia, G., and Menissier-de Murcia, J. (1992) The human poly(ADP-ribose) polymerase nuclear localization signal is a bipartite element functionally separate from DNA binding and catalytic activity. *EMBO J. 11*, 3263−3269.

(15) Langelier, M. F., Servent, K. M., Rogers, E. E., and Pascal, J. M. (2008) A third zinc-binding domain of human poly(ADP-ribose) polymerase-1 coordinates DNA-dependent enzyme activation. *J. Biol. Chem. 283*, 4105−4114.

(16) Tao, Z., Gao, P., Hoffman, D. W., and Liu, H.-W. (2008) Domain C of human poly(ADP-ribose) polymerase-1 is important for enzyme activity and contains a novel zinc-ribbon motif. *Biochemistry 47*, 5804−5813.

(17) Bork, P., Hofmann, K., Bucher, P., Neuwald, A. F., Altschul, S. F., and Koonin, E. V. (1997) A superfamily of conserved domains in DNA damage-responsive cell cycle checkpoint proteins. *FASEB J. 11*, 68−76.

(18) Semighini, C. P., Savoldi, M., Goldman, G. H., and Harris, S. D. (2006) Functional characterization of the putative *Aspergillus nidulans* poly(ADP-ribose) polymerase homolog PrpA. *Genetics 173*, 87−98.

(19) Huambachano, O., Herrera, F., Rancourt, A., and Satoh, M. S. (2011) Double-stranded DNA binding domain of poly(ADP-ribose) polymerase-1 and molecular insight into the regulation of its activity. *J. Biol. Chem. 286*, 7149−7160.

(20) Ruf, A., de Murcia, G., and Schulz, G. E. (1998) Inhibitor and NAD^+ binding to poly(ADP-ribose) polymerase as derived from crystal structures and homology modeling. *Biochemistry 37*, 3893−3900.

(21) Simonin, F., Höfferer, L., Panzeter, P. L., Muller, S., de Murcia, G., and Althaus, F. R. (1993) The carboxyl-terminal domain of human poly(ADP-ribose) polymerase. Overproduction in *Escherichia coli*, large scale purification, and characterization. *J. Biol. Chem. 268*, 13454−13461.

(22) Langelier, M. F., Planck, J. L., Roy, S., and Pascal, J. M. (2011) Crystal structures of poly(ADP-ribose) polymerase-1 (PARP-1) zinc fingers bound to DNA: Structural and functional insights into DNA-dependent PARP-1 activity. *J. Biol. Chem. 286*, 10690−10701.

(23) Hattori, K., Kido, Y., Yamamoto, H., Ishida, J., Kamijo, K., Murano, K., Ohkubo, M., Kinoshita, T., Iwashita, A., Mihara, K., Yamazaki, S., Matsuoka, N., Teramura, Y., and Miyake, H. (2004) Rational approaches to discovery of orally active and brain-penetrable quinazolinone inhibitors of poly(ADP-ribose)polymerase. *J. Med. Chem. 47*, 4151−4154.

(24) Kinoshita, T., Nakanishi, I., Warizaya, M., Iwashita, A., Kido, Y., Hattori, K., and Fujii, T. (2004) Inhibitor-induced structural change of the active site of human poly(ADP-ribose) polymerase. *FEBS Lett. 556*, 43−46.

(25) Iwashita, A., Hattori, K., Yamamoto, H., Ishida, J., Kido, Y., Kamijo, K., Murano, K., Miyake, H., Kinoshita, T., Warizaya, M., Ohkubo, M., Matsuoka, N., and Mutoh, S. (2005) Discovery of quinazolinone and quinoxaline derivatives as potent and selective poly(ADP-ribose) polymerase-1/2 inhibitors. *FEBS Lett. 579*, 1389−1393.

(26) Miyashiro, J., Woods, K. W., Park, C. H., Liu, X., Shi, Y., Johnson, E. F., Bouska, J. J., Olson, A. M., Luo, Y., Fry, E. H., Giranda, V. L., and Penning, T. D. (2009) Synthesis and SAR of novel tricyclic quinoxalinone inhibitors of poly(ADP-ribose)polymerase-1 (PARP-1). *Bioorg. Med. Chem. Lett. 19*, 4050−4054.

(27) Penning, T. D., Zhu, G. D., Gong, J., Thomas, S., Gandhi, V. B., Liu, X., Shi, Y., Klinghofer, V., Johnson, E. F., Park, C. H., Fry, E. H., Donawho, C. K., Frost, D. J., Buchanan, F. G., Bukofzer, G. T., Rodriguez, L. E., Bontcheva-Diaz, V., Bouska, J. J., Osterling, D. J., Olson, A. M., Marsh, K. C., Luo, Y., and Giranda, V. L. (2010) Optimization of phenyl-substituted benzimidazole carboxamide poly(ADP-ribose) polymerase inhibitors: Identification of (*S*)-2-(2-fluoro-4-(pyrrolidin-2-yl)phenyl)-1*H*-benzimidazole-4-carboxamide (A-966492), a highly potent and efficacious inhibitor. *J. Med. Chem. 53*, 3142−3153.

(28) Gandhi, V. B., Luo, Y., Liu, X., Shi, Y., Klinghofer, V., Johnson, E. F., Park, C., Giranda, V. L., Penning, T. D., and Zhu, G. D. (2010) Discovery and SAR of substituted 3-oxoisoindoline-4-carboxamides as potent inhibitors of poly(ADP-ribose) polymerase (PARP) for the treatment of cancer. *Bioorg. Med. Chem. Lett. 20*, 1023−1026.

(29) Langelier, M. F., Planck, J. L., Roy, S., and Pascal, J. M. (2012) Structural basis for DNA damage-dependent poly(ADP-ribosyl)ation by human PARP-1. *Science 336*, 728−732.

(30) Mertens, H. D., and Svergun, D. I. (2010) Structural characterization of proteins and complexes using small-angle X-ray solution scattering. *J. Struct. Biol. 172*, 128−141.

(31) Berger, N. A., and Petzold, S. J. (1985) Identification of minimal size requirements of DNA for activation of poly(ADP-ribose) polymerase. *Biochemistry 24*, 4352−4355.

(32) Konarev, P. V., Volkov, V. V., Sokolova, A. V., Koch, M. H. J., and Svergun, D. I. (2003) PRIMUS: A Windows PC-based system for small-angle scattering data analysis. *J. Appl. Crystallogr. 36*, 1277−1282.

(33) Svergun, D. I. (1992) Determination of the regularization parameter in indirect-transform methods using perceptual criteria. *J. Appl. Crystallogr. 25*, 495−503.
(34) Svergun, D. I. (1999) Restoring low resolution structure of biological macromolecules from solution scattering using simulated annealing. *Biophys. J. 76*, 2879−2886.
(35) Petoukhov, M. V., Franke, D., Shkumatov, A. V., Tria, G., Kikhney, A. G., Gajda, M., Gorba, C., Mertens, H. D. T., Konarev, P. V., and Svergun, D. I. (2012) New developments in the ATSAS program package for small-angle scattering data analysis. *J. Appl. Crystallogr. 45*, 342−350.
(36) Maupetit, J., Gautier, R., and Tuffery, P. (2006) SABBAC: Online Structural Alphabet-based protein BackBone reconstruction from Alpha-Carbon trace. *Nucleic Acids Res. 34* (Web Server Issue), W147−W151.
(37) Phillips, J. C., Braun, R., Wang, W., Gumbart, J., Tajkhorshid, E., Villa, E., Chipot, C., Skeel, R. D., Kalé, L., and Schulten, K. (2005) Scalable molecular dynamics with NAMD. *J. Comput. Chem. 26*, 1781−1802.
(38) Lilyestrom, W., van der Woerd, M. J., Clark, N., and Luger, K. (2010) Structural and biophysical studies of human PARP-1 in complex with damaged DNA. *J. Mol. Biol. 395*, 983−994.
(39) Kozin, M., and Svergun, D. (2000) Automated matching of high- and low-resolution structural models. *J. Appl. Crystallogr. 34*, 33−41.
(40) Macke, T., and Case, D. A. (1998) Modeling unusual nucleic acid structures. In *Molecular Modeling of Nucleic Acids*, pp 379−393, American Chemical Society, Washington DC.
(41) Tao, Z., Gao, P., and Liu, H.-W. (2009) Identification of the ADP-ribosylation sites in the PARP-1 automodification domain: Analysis and implications. *J. Am. Chem. Soc. 131*, 14258−14260.
(42) Marsischky, G. T., Wilson, B. A., and Collier, R. J. (1995) Role of glutamic acid 988 of human poly-ADP-ribose polymerase in polymer formation. Evidence for active site similarities to the ADP-ribosylating toxins. *J. Biol. Chem. 270*, 3247−3254.
(43) Loeffler, P. A., Cuneo, M. J., Mueller, G. A., DeRose, E. F., Gabel, S. A., and London, R. E. (2011) Structural studies of the PARP-1 BRCT domain. *BMC Struct. Biol. 11*, 37.
(44) Trucco, C., Flatter, E., Fribourg, S., de Murcia, G., and Ménissier-de Murcia, J. (1996) Mutations in the amino-terminal domain of the human poly(ADP-ribose) polymerase that affect its catalytic activity but not its DNA binding capacity. *FEBS Lett. 399*, 313−316.
(45) Gradwohl, G., Ménissier de Murcia, J. M., Molinete, M., Simonin, F., Koken, M., Hoeijmakers, J. H., and de Murcia, G. (1990) The second zinc-finger domain of poly(ADP-ribose) polymerase determines specificity for single-stranded breaks in DNA. *Proc. Natl. Acad. Sci. U.S.A. 87*, 2990−2994.
(46) Ikejima, M., Noguchi, S., Yamashita, R., Ogura, T., Sugimura, T., Gill, D. M., and Miwa, M. (1990) The zinc fingers of human poly(ADP-ribose) polymerase are differentially required for the recognition of DNA breaks and nicks and the consequent enzyme activation. Other structures recognize intact DNA. *J. Biol. Chem. 265*, 21907−21913.
(47) Eustermann, S., Videler, H., Yang, J. C., Cole, P. T., Gruszka, D., Veprintsev, D., and Neuhaus, D. (2011) The DNA-binding domain of human PARP-1 interacts with DNA single-strand breaks as a monomer through its second zinc finger. *J. Mol. Biol. 407*, 149−170.
(48) Miranda, E. A., Dantzer, F., O'Farrell, M., de Murcia, G., and de Murcia, J. M. (1995) Characterisation of a gain-of-function mutant of poly(ADP-ribose) polymerase. *Biochem. Biophys. Res. Commun. 212*, 317−325.
(49) Gagné, J. P., Moreel, X., Gagné, P., Labelle, Y., Droit, A., Chevalier-Paré, M., Bourassa, S., McDonald, D., Hendzel, M. J., Prigent, C., and Poirier, G. G. (2009) Proteomic investigation of phosphorylation sites in poly(ADP-ribose) polymerase-1 and poly-(ADP-ribose) glycohydrolase. *J. Proteome Res. 8*, 1014−1029.
(50) Lonskaya, I., Potaman, V. N., Shlyakhtenko, L. S., Oussatcheva, E. A., Lyubchenko, Y. L., and Soldatenkov, V. A. (2005) Regulation of poly(ADP-ribose) polymerase-1 by DNA structure-specific binding. *J. Biol. Chem. 280*, 17076−17083.
(51) de Murcia, G., and Menissier de Murcia, J. (1994) Poly(ADP-ribose) polymerase: A molecular nick-sensor. *Trends Biochem. Sci. 19*, 172−176.
(52) Menissier de Murcia, J., Molinete, M., Gradwohl, G., Simonin, F., and de Murcia, G. (1989) Zinc-binding domain of poly(ADP-ribose)polymerase participates in the recognition of single strand breaks on DNA. *J. Mol. Biol. 210*, 229−233.
(53) Smulson, M. E., Pang, D., Jung, M., Dimtchev, A., Chasovskikh, S., Spoonde, A., Simbulan-Rosenthal, C., Rosenthal, D., Yakovlev, A., and Dritschilo, A. (1998) Irreversible binding of poly(ADP)ribose polymerase cleavage product to DNA ends revealed by atomic force microscopy: Possible role in apoptosis. *Cancer Res. 58*, 3495−3498.
(54) Pion, E., Bombarda, E., Stiegler, P., Ullmann, G. M., Mely, Y., de Murcia, G., and Gerard, D. (2003) Poly(ADP-ribose) polymerase-1 dimerizes at a 5′ recessed DNA end in vitro: A fluorescence study. *Biochemistry 42*, 12409−12417.
(55) Potaman, V. N., Shlyakhtenko, L. S., Oussatcheva, E. A., Lyubchenko, Y. L., and Soldatenkov, V. A. (2005) Specific binding of poly(ADP-ribose) polymerase-1 to cruciform hairpins. *J. Mol. Biol. 348*, 609−615.
(56) Chasovskikh, S., Dimtchev, A., Smulson, M., and Dritschilo, A. (2005) DNA transitions induced by binding of PARP-1 to cruciform structures in supercoiled plasmids. *Cytometry, Part A 68*, 21−27.
(57) Krishnakumar, R., Gamble, M. J., Frizzell, K. M., Berrocal, J. G., Kininis, M., and Kraus, W. L. (2008) Reciprocal binding of PARP-1 and histone H1 at promoters specifies transcriptional outcomes. *Science 319*, 819−821.
(58) Messner, S., Schuermann, D., Altmeyer, M., Kassner, I., Schmidt, D., Schär, P., Müller, S., and Hottiger, M. O. (2009) Sumoylation of poly(ADP-ribose) polymerase 1 inhibits its acetylation and restrains transcriptional coactivator function. *FASEB J. 23*, 3978−3989.
(59) Hassa, P. O., Haenni, S. S., Buerki, C., Meier, N. I., Lane, W. S., Owen, H., Gersbach, M., Imhof, R., and Hottiger, M. O. (2005) Acetylation of poly(ADP-ribose) polymerase-1 by p300/CREB-binding protein regulates coactivation of NF-kB-dependent transcription. *J. Biol. Chem. 280*, 40450−40464.
(60) Altmeyer, M., Messner, S., Hassa, P. O., Fey, M., and Hottiger, M. O. (2009) Molecular mechanism of poly(ADP-ribosyl)ation by PARP1 and identification of lysine residues as ADP-ribose acceptor sites. *Nucleic Acids Res. 37*, 3723−3738.
(61) Rajamohan, S. B., Pillai, V. B., Gupta, M., Sundaresan, N. R., Birukov, K. G., Samant, S., Hottiger, M. O., and Gupta, M. P. (2009) SIRT1 promotes cell survival under stress by deacetylation-dependent deactivation of poly(ADP-ribose) polymerase 1. *Mol. Cell. Biol. 29*, 4116−4129.
(62) Kauppinen, T. M., Chan, W. Y., Suh, S. W., Wiggins, A. K., Huang, E. J., and Swanson, R. A. (2006) Direct phosphorylation and regulation of poly(ADP-ribose) polymerase-1 by extracellular signal-regulated kinases 1/2. *Proc. Natl. Acad. Sci. U.S.A. 103*, 7136−7141.